



HAL
open science

Optimisation of the filter housing dimensions of an automatic flushing strainer-type filter

Nicolás Cano, Antonio Pires de Camargo, Nassim Ait-Mouheb, Gustavo Lopes Muniz, Jhonnatan Alexander Yepes Guarnizo, Diego José de Sousa Pereira, José Frizzone

► To cite this version:

Nicolás Cano, Antonio Pires de Camargo, Nassim Ait-Mouheb, Gustavo Lopes Muniz, Jhonnatan Alexander Yepes Guarnizo, et al.. Optimisation of the filter housing dimensions of an automatic flushing strainer-type filter. *Biosystems Engineering*, 2022, 219, pp.25-37. 10.1016/j.biosystemseng.2022.04.019 . hal-03651452

HAL Id: hal-03651452

<https://hal.science/hal-03651452v1>

Submitted on 25 Apr 2022

HAL is a multi-disciplinary open access archive for the deposit and dissemination of scientific research documents, whether they are published or not. The documents may come from teaching and research institutions in France or abroad, or from public or private research centers.

L'archive ouverte pluridisciplinaire **HAL**, est destinée au dépôt et à la diffusion de documents scientifiques de niveau recherche, publiés ou non, émanant des établissements d'enseignement et de recherche français ou étrangers, des laboratoires publics ou privés.

Biosystems Engineering

Optimisation of the filter housing dimensions of an automatic flushing strainer-type filter --Manuscript Draft--

Manuscript Number:	YBENG-D-21-00970R2
Article Type:	Research Paper
Keywords:	filtration; CFD; screen filter; irrigation engineering; hydraulics
Corresponding Author:	Antonio Pires de Camargo, PhD Faculdade de Engenharia Agrícola - FEAGRI/UNICAMP Campinas, SP Brazil
First Author:	Nicolás Duarte Cano, MSc
Order of Authors:	Nicolás Duarte Cano, MSc Antonio Pires de Camargo, PhD Nassim Ait-Mouheb, PhD Gustavo Lopes Muniz Jhonnatan Alexander Yepes Guarnizo Diego José de Sousa Pereira José Antônio Frizzzone
Manuscript Region of Origin:	South America
Abstract:	<p>Filtration is essential in drip irrigation systems to remove physical contaminants carried by water that can clog the emitters, cause wear, or foul components of the system, affecting its performance and lifespan. Automatic flushing strainer-type filters initiate and terminate discrete flushing cycles that are activated automatically by means of differential pressure. The objective of this study is to investigate the hydraulic performance and flow behaviour of an automatic flushing strainer-type filter operated with clean water, using experimental and numerical approaches, to optimise the dimensions of its filter housing and to increase the range of operating flow rates. Pressure drop curves were determined for the filter housing and the filter system equipped with five models of filter elements (woven and non-woven elements). Excessive pressure drop in the filter housing and low filtration rates were identified as the main drawbacks of the original filter system. Numerical simulations enabled the identification of the most critical regions in terms of pressure losses near the transitions between the inlet and outlet segments of the pipe. Four designs of filter housing were simulated to evaluate the possibilities of optimising the filter housing dimensions using a constant filtering area. Larger inlet and outlet diameters combined to a filter housing shorter and wider were improvements in the filter housing dimensions that enabled to decrease the pressure drop in the filter and/or increase the range of operating flow rates. The results provided useful information for enhancing the hydraulic performance of the filtration system.</p>
Opposed Reviewers:	
Response to Reviewers:	

Declaration of interests

The authors declare that they have no known competing financial interests or personal relationships that could have appeared to influence the work reported in this paper.

The authors declare the following financial interests/personal relationships which may be considered as potential competing interests:

Highlights

- An automatic flushing strainer-type filter and five filter elements were studied
- Excessive pressure losses were caused by the filter housing design
- Four designs of filter housing were investigated by numerical approaches
- CFD enabled to investigate fluid flow and to optimise the filter housing dimensions
- Improvements enabled to improve the hydraulic performance of the filter housing

1 **Optimisation of the filter housing dimensions of an automatic flushing strainer-**
2 **type filter**

3
4 Nicolas D. Cano ^a; Antonio P. Camargo ^b; Nassim Ait-Mouheb ^c; Gustavo L. Muniz ^d; Jhonnatan A. Y.
5 Guarnizo ^e; Diego J. S. Pereira ^f; José A. Frizzone^g
6

7 ^a Ph.D Student, Agricultural Engineering College, University of Campinas, Campinas, SP 13083-970,
8 Brazil. ORCID: <https://orcid.org/0000-0002-1649-3060>. Email: n181139@dac.unicamp.br

9 ^b Professor, Agricultural Engineering College, University of Campinas, Campinas, Brazil. ORCID:
10 <https://orcid.org/0000-0001-5164-2634>. Email: apcpires@unicamp.br (Corresponding author)

11 ^c INRAE, UMR G-EAU, University of Montpellier, Avenue Jean-François Breton, 34000 Montpellier,
12 France. ORCID: <https://orcid.org/0000-0003-0099-0983>. Email: nassim.ait-mouheb@inrae.fr

13 ^d Ph.D Student, Agricultural Engineering College, University of Campinas, Campinas, SP, Brazil.
14 ORCID: <https://orcid.org/0000-0002-6045-611X>. Email: gustavo.muniz@feagri.unicamp.br

15 ^e Ph.D Student, Agricultural Engineering College, University of Campinas, Campinas, SP 13083-970,
16 Brazil. ORCID: <https://orcid.org/0000-0001-9313-9834> Email: j261219@dac.unicamp.br

17 ^f Ph.D Student, Biosystems Engineering Department, University of São Paulo, College of Agriculture
18 “Luiz de Queiroz”, Piracicaba, SP, Brazil. ORCID: <https://orcid.org/0000-0002-0160-0249> Email:
19 dpereira@usp.br

20 ^g Professor, Dept. of Biosystems Engineering, College of Agriculture “Luiz de Queiroz,” Univ. of São
21 Paulo, Piracicaba, SP 13418-900, Brazil. ORCID: <https://orcid.org/0000-0002-4251-1496>. Email:
22 frizzone@usp.br

23 **Abstract:** Filtration is essential in drip irrigation systems to remove physical
24 contaminants carried by water that can clog the emitters, cause wear, or foul
25 components of the system, affecting its performance and lifespan. Automatic flushing
26 strainer-type filters initiate and terminate discrete flushing cycles that are activated
27 automatically by means of differential pressure. The objective of this study is to
28 investigate the hydraulic performance and flow behaviour of an automatic flushing
29 strainer-type filter operated with clean water, using experimental and numerical
30 approaches, to optimise the dimensions of its filter housing and to increase the range of
31 operating flow rates. Pressure drop curves were determined for the filter housing and the
32 filter system equipped with five models of filter elements (woven and non-woven
33 elements). Excessive pressure drop in the filter housing and low filtration rates were
34 identified as the main drawbacks of the original filter system. Numerical simulations
35 enabled the identification of the most critical regions in terms of pressure losses near the
36 transitions between the inlet and outlet segments of the pipe. Four designs of filter
37 housing were simulated to evaluate the possibilities of optimising the filter housing
38 dimensions using a constant filtering area. Larger inlet and outlet diameters combined to
39 a filter housing shorter and wider were improvements in the filter housing dimensions
40 that enabled to decrease the pressure drop in the filter and/or increase the range of
41 operating flow rates. The results provided useful information for enhancing the
42 hydraulic performance of the filtration system.

43 **Keywords:** filtration; CFD; screen filter; irrigation engineering; hydraulics

44 **Nomenclature**

A	Total surface area of filtration (mm^2)
a, b	Fitted coefficients of the pressure drop equation
CFD	Computational fluid dynamics

D	Inlet diameter of the filter (mm)
D_{el}	Diameter of the filter element (mm)
D_{ho}	Diameter of the filter housing (mm)
h_{he}	Height of the filter element (mm)
h_{ho}	Height of the filter housing (mm)
NW	Nonwoven
PP	Polypropylene
Q	Flow rate ($\text{m}^3 \text{h}^{-1}$)
q	Filtration rate ($\text{m}^3 \text{m}^{-2} \text{h}^{-1}$)
Q_n	Nominal flow rate ($\text{m}^3 \text{h}^{-1}$)
R^2	Coefficient of determination
SS	Stainless steel
y^+	Dimensionless wall distance
Δp	Differential pressure (kPa)
Δp_{exp}	Differential pressure for the original filter housing, obtained experimentally (kPa)
Δp_f	Differential pressure of the filter element (kPa)
$\Delta p_{housing}$	Differential pressure of the filter housing (kPa)
Δp_{sim}	Differential pressure for the original filter housing, obtained by numerical simulation (kPa)
Δp_{total}	Differential pressure of the filter system (filter housing and element) (kPa)

45

46

47

48 **1 Introduction**

49 Filtration involves the physical separation of one or more components from a
50 suspension in a fluid by passage through or across a barrier (filter medium) that is
51 permeable only to some of these components (Purchas & Sutherland, 2002). In
52 irrigation systems, particularly in microirrigation, filtration is important to prevent the
53 intake of particles and sediments that can accumulate along pipes and other
54 components, resulting in the clogging of emitters. Under typical irrigation conditions,
55 complete removal of all suspended particles cannot be achieved (ISO9912-1, 2004).
56 Practical and economic limitations only allow for the removal of larger particles, and
57 consequently, sediments can be found in irrigation lines (Oliveira et al., 2020; Puig-
58 Bargués & Lamm, 2013; Ravina et al., 1992)

59 Strainer-type, or screen filters, are devices that contain one or more filter elements. The
60 strainer-type filter elements consist of a perforated plate, screen, mesh, or a combination
61 of these, intended to retain suspended solids larger than the aperture size specified by
62 the manufacturer. The screen can be made of steel, nylon, polypropylene, or nonwoven
63 materials. The material and characteristics of the screen directly affect the fluid flow
64 and performance of the filter (Sparks & Chase, 2016; Sutherland, 2008). In irrigation
65 applications, the filter performance mainly refers to hydraulic performance (i.e.,
66 pressure drop, filtration rate), removal efficiency of suspended particles, resistance to
67 corrosion, and backwash effectiveness when automatic mechanisms are part of the
68 filtration system. For woven wire cloths, the filtration performance is influenced by
69 filter cloth specifications such as wire diameter, shape and material, type of weave (e.g.,
70 plain Dutch weave, twill Dutch weave, reverse Dutch weave), aperture size, and mesh
71 count. The performance of nonwoven fabrics is influenced by the material, porosity,
72 permeability, thickness, pore size, and mass per unit area of the fabric (Ribeiro et al.,

73 2004, 2008). For media filters, the requirements for evaluating several characteristics
74 related to filter performance are standardized in ASAE S539 (ASABE, 2017).

75 The filtration for irrigation systems may consist of primary and secondary filters. The
76 primary filter may serve several plots and consist of a media filter, screen or disc filter,
77 most often incorporating a self-cleaning mechanism. Screen or disc filters manually
78 cleaned, can be installed as secondary downstream safety filters at the inlet of plots
79 (Pizarro Cabello, 1996; Ravina et al., 1997). Screen filters are suitable for removing
80 suspended solid particles, but problems may arise when algal debris are part of the
81 contaminants. Algal material tends to intertwine between the screen mesh and removal
82 is difficult when the packing becomes dense (Nakayama et al., 2007). If the irrigation
83 water contains a high concentration of suspended solid particles, sand separators or
84 settling basins should be installed upstream of the filtration system (Keller & Bliesner,
85 2000).

86 Some screen filters have flushing cycles that are automatically activated, and they are
87 called automatic flushing strainer-type filters (ISO9912-3, 2013). Automatic flushing
88 filters initiate and terminate discrete flushing cycles that are activated automatically by
89 means of differential pressure or at regular intervals of time or filtered volume
90 (Nakayama et al., 2007).

91 Several studies have emerged in recent years with the intention of improving designs for
92 energy consumption, and understanding the flow behaviour and performance of filters,
93 mainly media filters (Arbat et al., 2011; Bové et al., 2017; Bové, Arbat, Pujol, et al.,
94 2015; Mesquita et al., 2017, 2019; Pujol et al., 2020; Solé-Torres et al., 2019). Many
95 studies have used computational fluid dynamics (CFD) to investigate, design, and
96 improve irrigation equipment (Camargo et al., 2020). Although experimental data will
97 always be necessary for the validation of numerical simulations and to confirm the

98 performance of irrigation equipment, numerical simulations can be useful to reduce
99 resources related to development costs.

100 Mathematical models based on dimensional analysis have been developed to predict
101 head losses of filters for irrigation systems operated with tap water (Yurdem et al.,
102 2008, 2010), water with suspended solids, and effluents (Duran-Ros et al., 2010; Puig-
103 Bargués et al., 2005; Zong et al., 2015). Some of these models can describe filter
104 clogging as a function of the characteristics of the filter, water, and flow. CFD was used
105 to estimate fluid flow characteristics and pressure losses in different parts of sand filters,
106 as well as to propose improvements in the design of filter components aiming for better
107 hydraulic performance (Arbat et al., 2011; Bové, Arbat, Pujol, et al., 2015; Mesquita et
108 al., 2017, 2019). CFD studies on strainer-type filters are scarce in the literature on
109 irrigation engineering.

110 The objective of this study was to investigate the hydraulic performance and flow
111 behaviour of an automatic flushing strainer-type filter operated with clean water, using
112 experimental and numerical approaches, to optimise the dimensions of its filter housing
113 and to increase the range of operating flow rates.

114 **2 Material and methods**

115 **2.1 Filter**

116 The automatic flushing strainer-type filter model FA-20 manufactured by Iavant
117 Filtering Systems, Brazil, was investigated (Fig. 1). The filter housing is made of steel,
118 and an electrostatic powder coating is applied over its inner and outer surfaces. The inlet
119 and outlet internal diameters are 80 mm, and the total surface area of the filtration
120 element is 272,376 mm².

121 This filtration system operates differently from other automatic flushing strainer-type
122 filters. In this filter, the operating water flows from the outer to the inner surface of the

123 filter element; thus, residues gradually accumulate over the external surface of the
 124 element. The automatic flushing mechanism is activated by a differential pressure
 125 threshold with a default value of 50 kPa. When the flushing routine is activated, the
 126 flushing valve is opened, and the electric motor coupled to a gearbox rotates the filter
 127 element. When the filter element rotates, its outer surface rubs against the brushes,
 128 which facilitates the detachment of solid material accumulated during the filtration
 129 routine. Parallel to the brushes, there is a narrow cavity that is connected to a flushing
 130 pipe. The differential pressure between the inside of the filter and the atmosphere is
 131 converted into a high velocity through the flushing pipe, which removes the material
 132 accumulated over the external surface of the filter element.

133 **[Fig. 1]**

134 A technical description of the five models of the filter elements evaluated is presented in
 135 Table 1. According to the filter manufacturer, stainless steel (SS-120 and SS-150) and
 136 polypropylene (PP-120) models are used in several applications (e.g., irrigation,
 137 wastewater, water supply, and industry), whereas non-woven models (NW-500 and
 138 NW-2500) are usually required for industrial purposes. Fig. 2 shows images of the
 139 woven and non-woven meshes obtained using a Leica M125C stereo microscope.

140 **Table 1.** Specifications of the filter elements provided by the mesh manufacturers.

Model	Material	Mesh count	Aperture size (μm)	Type of weave	Additional specifications
SS-120	Stainless steel	120	125	Plain Dutch weave	Wire diameter: 0.38 mm (warp) and 0.26 mm (weft); Number of apertures per inch: 24 (warp) and 110 (weft). Number approx. of apertures per cm 9 (warp) and 43 (weft)
SS-150	Stainless steel	150	100	Plain Dutch weave	Wire diameter: 0.23 mm (warp) and 0.18 mm (weft); Number of apertures per inch: 30 (warp) and 150 (weft). Number approx. of apertures per cm 12 (warp) and 59 (weft)
PP-120	Polypropylene	120	125	Satim weave, calendered, monofilament	Wire diameter: 0.64 mm; Mass per unit area: 300 g m^{-2} ; Air permeability: $80 \text{ m}^3 \text{ m}^{-2} \text{ min}^{-1}$ at 200 Pa
NW-500	Polypropylene	500	25	Non-woven, needlona® PP/PP	Air permeability: $13 \text{ m}^3 \text{ m}^{-2} \text{ min}^{-1}$ at 200 Pa

141

142

[Fig. 2]

143 2.2 Experimental set-up

144 Tests were carried out at the Hydraulics and Irrigation Laboratory (LHI/FEAGRI/
145 UNICAMP), Campinas, SP, Brazil.

146 The pressure drop curves as a function of flow rate were determined in the test bench, as
147 illustrated in Fig. 3 using clean tap water. The hydraulically closed circuit consisted of a
148 25 m³ water tank, a 18.6 kW centrifugal pump (maximum flow rate of 70 m³ h⁻¹ at 400
149 kPa), an orifice plate flow meter equipped with a differential pressure transmitter,
150 calibrated in the range from 20 to 65 m³ h⁻¹ (maximum error of 5% from the measured
151 value), a gate valve installed upstream of the filter to set the testing pressure, a
152 temperature transmitter PT100 (0 to 50 °C, maximum error of 0.5 °C), a pressure
153 transmitter (0 to 500 kPa, maximum error of 0.5% of the full scale), a differential
154 pressure transmitter (0 to 100 kPa, maximum error of 0.5% of the full scale), the filter
155 under test, and a gate valve installed downstream of the filter to adjust the test flow rate.
156 The pressure tap distance was 5 *D* at the filter inlet and 10 *D* at the filter outlet
157 (ASABE, 2017; ISO9644, 2008).

158

[Fig. 3]

159 All sensors provided an analogue output signal that ranged from 4 to 20 mA, which
160 varied linearly with the measured quantity. The data acquisition of all measurement
161 instruments was performed using an electronic system equipped with a 16-bit analogue-
162 to-digital converter to acquire analogue signals within the range of 4 to 20 mA and a
163 resolution of 625 nA. The differential pressure was measured increasing and decreasing
164 conditions of flow rate. For each test condition, 100 records of the sensor readings. were

165 sampled at a 1 s acquisition interval. Data was gathered in three replications evaluating
166 one unit of each filter element model.
167 Pressure drop curves as a function of flow rate were determined for the filter housing
168 without filter elements, as well as for the filter system equipped with each of the filter
169 elements shown in Table 1. The pressure drop in the filter was measured at flow rates
170 varying from 25 to 65 m³ h⁻¹. The pressure at the filter inlet ranged from 350 to 400
171 kPa, and the average water temperature was 21.5 °C (20.7 and 22.5 °C were the extreme
172 values). The automatic flushing mechanism was disabled during the experiments
173 because it was not part of the purpose of this study.

174 **2.3 Simulations evaluating the original filter housing**

175 CFD simulations were performed to estimate the pressure drop of the original filter
176 housing operated with clean water. In this stage, experimental data of pressure drop as a
177 function of flow rate was available for comparison. Numerical simulations including
178 filter elements were not included in this study.

179 The CFD module of COMSOL Multiphysics V. 5.4. was used to draw the three-
180 dimensional solids representing the filter housing and running the numerical
181 simulations. Simulations assumed an incompressible Newtonian fluid (i.e., water) and
182 steady state conditions.

183 The realisable k- ϵ model was used to solve the turbulent flow. This model is an
184 extension to the standard k- ϵ model which is used for simulating incompressible and
185 single-phase flows at high Reynolds numbers (COMSOL Multiphysics, 2016).

186 Comparison of turbulence models was not part of the study. Log-law wall functions
187 were applied to approximate the flow velocity profile inside the boundary layer, serving
188 to bridge the velocity profile from the wall to the main flow. The no-slip condition was
189 assumed.

190 Simulations were performed for three flow rates corresponding to some of the
191 conditions in which experimental data was available: 35.7, 49.5 and 62.8 m³ h⁻¹. Taking
192 the inlet diameter as a reference dimension, the Reynolds number varied from 162,099
193 to 285,149, indicating turbulent flow conditions in all simulations. The mean flow
194 velocity corresponding to each flow rate was set as a boundary condition at the filter
195 inlet, and the pressure was set to 400 kPa as a boundary condition at the filter outlet.
196 The mesh was generated based on the free tetrahedrals, including a boundary layer mesh
197 (i.e., inflation or prism layer) near the walls (Fig. 4). The default values were kept for
198 the boundary layer mesh (number of layers = 5; stretching factor = 1.2; thickness of first
199 layer = automatic; thickness adjustment factor = 2.5).

200 [Fig. 4]

201 The mesh quality was examined based on minimum and average element quality
202 (skewness). Mesh independence analysis was performed to validate the simulations.
203 Velocity profiles were plotted at four flow sections (inlet pipe, middle of the filter
204 housing, outlet of the filter housing, and outlet pipe) and results of pressure drop in the
205 filter were analysed to prove the results were mesh independent.

206 **2.4 Simulations for optimizing the filter housing dimensions**

207 Excessive pressure drop in the filter housing and low filtration rates were identified as
208 the main drawbacks in the original filter system; hence, simulations focused on
209 evaluating possibilities for optimizing the filter housing dimensions.

210 Four designs of the filter housing were simulated (Fig. 5). The total surface area of the
211 filtration was kept constant in all the designs ($A = 272,376 \text{ mm}^2$). The inlet and outlet
212 diameters of the filter housing were the basic dimensions of the new designs and were
213 set according to the commercial diameters of the steel pipes (80, 100, 125, and 150
214 mm).

215 The steps to obtain the main dimensions of the filter housing were as follows: 1) Define
216 the inlet diameter (D); 2) Filter element diameter ($D_{el} = D + 90$); 3) Filter housing
217 diameter ($D_{ho} = D_{el} + 40$); 4) Filter element height ($h_{el} = \frac{A}{\pi D_{el}}$); 5) 5: Filter housing
218 height ($h_{ho} = h_{el} + 160$). The values summed to each of the variables were based on
219 the dimensions measured in the original filter housing. Model A (80 mm) corresponded
220 to the original filter housing dimensions, but inlet and outlet pipes were changed to 150
221 mm and reducing adapters were added, as explained below.

222 [Fig. 5]

223 For optimising the filter housing dimensions, the maximum filtration rate $375 \text{ m}^3 \text{ m}^{-2} \text{ h}^{-1}$
224 found in commercial automatic flushing strainer-type filters (AMIAD, 2022; AZUD,
225 2022; NETAFIM, 2022) was assumed as the target value (see discussion in section 3.1).
226 For a total surface area of $272,376 \text{ mm}^2$, the corresponding flow rate for the automatic
227 flushing strainer-type filter was $102.1 \text{ m}^3 \text{ h}^{-1}$. Therefore, a pressure of 400 kPa at the
228 filter outlet and the flow rate of $100 \text{ m}^3 \text{ h}^{-1}$ were set as boundary conditions for CFD
229 simulations. Also, pipes of 150 mm diameter and reducing adapters were included at the
230 filter inlet and outlet in these simulations to keep flow velocities lower than 2 m s^{-1} in
231 the pipeline, as recommended in most of practical applications (Azevedo Netto &
232 Fernandez, 2015). Including the reducing adapters in the simulations enables to consider
233 minor losses caused by these fittings.

234 **3 RESULTS AND DISCUSSION**

235 **3.1 Pressure drop curves – Experimental data**

236 Figure 6 shows the pressure drop curves of the filtering system with and without the
237 filter elements. The pressure drop curve in filters is influenced by the geometric
238 characteristics of the filter housing and filter elements, as well as the filtering water

239 characteristics (Wu et al., 2014). In this stage, the filter housing and filtering water
240 quality were the same for all evaluations.

241 **[Fig. 6]**

242 The pressure drop curves of the woven filter elements SS-120, SS-150, and PP-120
243 were similar. These three models offer similar resistance to flow, although Table 1
244 indicates differences in aperture size, wire diameter, wire material, and type of weave of
245 these filter elements. Testezlaf and Ramos (1995) also found that the differences
246 between pressure drop curves of 125- and 100- μm screen filters were not significant
247 because of their similar permeability.

248 The pressure losses of 15 types of screen filters with plain weave woven wire cloth were
249 analysed by Wu et al. (2014). The plain weave filter cloth is one of the simplest weave
250 patterns, in which single wires (i.e., weft and warp wires) have the same diameter and
251 are woven together to form rectangular or square apertures. Wu et al. (2014) developed
252 an empirical model based on dimensional analysis to predict pressure losses in screen
253 filters was proposed. In their experiments, the filter pore and the wire diameters ranged
254 from 120.4 to 195.6 μm and 64.5 to 208.5 μm , respectively. For screen filters with 64.5
255 μm wire diameter, Wu et al. (2014) identified that the pressure drop increased when the
256 mesh count was increased from 80 mesh to 140 mesh (i.e., the aperture size decreased
257 from 200 to 115 μm), but the differences in pressure drop due to mesh count were not
258 statistically significant. Also, for a given mesh count, the increase in wire diameter
259 reduced the pore size and filter permeability and increased the pressure drop in the
260 filters. Given a fixed flow range and mesh count, a larger inlet/outlet diameter and a
261 thinner wire diameter of the screen reduced the inlet flow velocity and average filter
262 flow velocity minimising both head loss caused by pipeline turbulence and local head
263 loss caused by streams (Wu et al., 2014).

264 The pressure drop in a clean strainer-type filter ranges from 10 to 30 kPa, and the filter
265 element should be cleaned when Δp reaches 40–60 kPa (Pizarro Cabello, 1996). In this
266 study, the nominal flow rate (Q_n) for a clean filter was calculated assuming a midrange
267 value of Δp , which was 20 kPa. The nominal flow rate ranged from 59.1 to 60.7 m³ h⁻¹
268 for the elements SS-120, SS-150, and PP-120 (Table 2). The difference in Q_n values
269 among these elements was less than 5%.

270 The pressure drop curves of the non-woven filter elements (i.e., NW-500 and NW-
271 2500) were steeper than those of the woven filter elements (i.e. SS-120, SS-150, and
272 PP-120), which is expected because the non-woven elements presented lower
273 permeability and offer higher resistance to flow than the woven elements. The lower
274 permeability of the non-woven elements also led to nominal flow rates that were
275 approximately 20% smaller than those of the woven elements. Comparing the non-
276 woven filter elements, the difference in Q_n was approximately 8%, although the air
277 permeability of NW-500 was more than three times that of NW-2500.

278 At the nominal flow rate, the pressure drop due to the filter housing in the woven
279 elements (i.e., SS-120, SS-150, and PP-120) was dominant and represented more than
280 87% of the total pressure drop in the filtering system (Table 2). In the non-woven filter
281 elements operating at the nominal flow rate, the pressure drop due to the filter housing
282 was more than 60% of the total pressure drop in the filtering system.

283 The percentages of pressure drop caused by the filter housing (Table 2) suggest that
284 enhancements in the filter housing design could improve energy efficiency aspects and,
285 perhaps, it could allow the filtering system to operate at higher flow rates (Demir et al.,
286 2009; Wu et al., 2014). Table 2 presents the pressure drop equations for each filter
287 element. These equations were estimated by the difference between the results of the

288 total pressure drop in the filtering system and the pressure drop caused by the original
 289 filter housing.

290 **Table 2.** Nominal flow rate, filtration rate and percentage of pressure drop caused by
 291 the original filter housing when the filtering system is operating at the nominal flow
 292 rate, and pressure drop equation of each filter element.

Model	Q_n ($\text{m}^3 \text{h}^{-1}$)	q ($\text{m}^3 \text{m}^{-2} \text{h}^{-1}$)	% of pressure drop caused by the filter housing at Q_n	Pressure drop equation of the filter element $\Delta p_{f(kPa)} = a Q^b_{(\text{m}^3 \text{h}^{-1})}$		
				a	b	R^2
SS-120	60.7	222.9	91.0	2.07E-5	2.79	0.992
SS-150	59.1	217.0	87.8	1.35E-4	2.41	0.997
PP-120	59.8	219.4	89.1	3.40E-4	2.15	0.999
NW-500	48.0	176.1	66.6	4.21E-2	1.31	0.999
NW-2500	44.4	162.8	60.0	8.08E-2	1.21	0.999

293 Q_n is the filtering system nominal flow rate predicted considering 20 kPa differential pressure; q is the filtration rate
 294 considering the total surface area of filtration and Q_n ; Δp_f is the pressure drop of the filter element alone; Q is the
 295 flow rate; R^2 is the coefficient of determination.

296

297 In irrigation, the filtration rate of strainer-type filters with elements made of steel woven
 298 wire mesh usually range from 446 to 1004 $\text{m}^3 \text{m}^{-2} \text{h}^{-1}$ (Pizarro Cabello, 1996). The flow
 299 rate can be obtained by multiplying the filtration rate by the total surface area of the
 300 filter element. For the stainless-steel elements evaluated (i.e., SS-120 and SS-150), the
 301 filtration rate at Q_n ranged from 217.0 to 222.9 $\text{m}^3 \text{m}^{-2} \text{h}^{-1}$. The filtration rate values
 302 indicated in Table 2 are smaller than the values reported in the literature, which suggests
 303 that the filtering system could operate at higher flow rates if the filter housing design
 304 was improved to reduce the pressure drop. Based on the values presented by Pizarro
 305 Cabello (1996) for steel woven wire mesh, the flow rate values can vary from 121.5 to
 306 273.5 $\text{m}^3 \text{h}^{-1}$ (i.e., 446 to 1004 $\text{m}^3 \text{m}^{-2} \text{h}^{-1}$).

307 If an increase in the flow rate does not interfere with the removal efficiency of solid
 308 particles, improvements in the filter housing design could contribute to enlarge the
 309 range of operating conditions of the filtration system, to reduce pressure losses and
 310 energy consumption. As examples to encourage further investigation on these aspects,

311 the 4" automatic vertical screen filter Netafim Screenguard™ exhibits a filtration
312 surface area of 0.2 m² and maximum recommended filtration rate of 375 m³ m⁻² h⁻¹
313 (NETAFIM, 2022); the 4" Azud Luxon MFH 2400 M/4 has a filtration surface area of
314 0.24 m² and maximum recommended filtration rate of 375 m³ m⁻² h⁻¹ (AZUD, 2022);
315 and the 4" Filtomat M104C exhibits a filtration surface area of 0.212 m² and maximum
316 recommended filtration rate of 377 m³ m⁻² h⁻¹ (AMIAD, 2022). The maximum filtration
317 rates recommended by the manufacturers of automatic flushing strainer-type filters are
318 lower than the values proposed by Pizarro Cabello (1996). Regardless of the type of
319 filter, lower filtration rates are recommended for low-quality water (Ravina et al., 1997).

320 **3.2 Simulated and experimental pressure losses of the original filter housing**

321 Simulations of the original filter housing were performed at flow rates of 35.7, 49.5 and
322 62.8 m³ h⁻¹. Mesh independence analyses were performed to validate all conditions
323 simulated. Figure 7 shows velocity profiles plotted at four flow sections (I, II, III and
324 IV) and results of pressure drop in the filter operating at 62.8 m³ h⁻¹, which corresponds
325 to 3.47 m s⁻¹ at the filter inlet. The influence of mesh size in the velocity profiles and
326 values of pressure drop in the filter housing is clearly demonstrated in Fig. 7. Mesh
327 independence was confirmed when the mesh size was increased from 4,053,468 (e) to
328 4,684,543 (f) elements. In these mesh sizes (e and f), the velocity profiles are
329 practically matching at the four flow sections evaluated, and the pressure drop in the
330 filter housing was 29.8 and 29.7 kPa, which represents a difference smaller than 0.5%.
331 Although not shown here, the same procedure was used for proving the results were
332 mesh independent in all CFD simulations.

333 Figure 7 also shows values of y^+ for the simulation at 62.8 m³ h⁻¹ using mesh size f, in
334 which mesh independence was identified. The distance between the first grid cell and
335 wall (y^+ , dimensionless wall distance) should be lower than an upper limit, which

336 depends on the Reynolds number (Pope, 2000). Log-law of wall provides a function for
337 velocity to match the inner sub-layer to the outer layer and is extensively verified
338 experimentally. The log-law wall functions are known to be valid for $30 < y^+ < 1,000$
339 (Tabatabaian, 2015). In COMSOL, log-law is used for wall functions up to $y^+ = 11.06$
340 for the k- ϵ model and y^+ is designated by δ_w^+ in the software documentation (COMSOL
341 Multiphysics, 2016; Tabatabaian, 2015).

342 In all simulations, the minimum element quality ranged from 0.065 to 0.1, and the
343 average element quality varied between 0.68 to 0.72. In COMSOL, the mesh quality of
344 1 represents an optimal element quality, while minimum element qualities below 0.01
345 are very low quality and should be avoided to prevent convergence problems.

346 **[Fig. 7]**

347 Figure 8 shows the experimental and simulated values of the pressure drop for the
348 original filter housing evaluated under mean flow velocities at the filter inlet 1.97, 2.73
349 and 3.47 m s⁻¹, which corresponds to flow rates of 35.7, 49.5 and 62.8 m³ h⁻¹,
350 respectively. Simulations overestimated the pressure drop in the filter housing as the
351 flow velocity was increased. Differences between measured and simulated values can be
352 attributed to the simplifications in the three-dimensional model, inaccuracies of the
353 turbulence flow model, and experimental data measurement uncertainty (Pope, 2000).
354 Ilker and Sorgun (2020) observed errors of up to 20% evaluating the performance of
355 different flow turbulence models for single-phase and liquid-solid slurry flows in
356 pressurized pipe systems. Movahedi and Jamshidi (2021) evaluated the accuracy of
357 different turbulence models for the prediction of pressure drop along with an annular
358 pipe and reported errors of up to 25% according to the model employed. For practical
359 purposes, to estimate how changes in the filter housing dimensions will influence the
360 filter pressure drop, we can assume the prediction errors are acceptable and useful.

361

[Fig. 8]

362 Part of the pressure drop found in filters is produced by the filter medium itself and
363 cannot be avoided. However, a large part of the pressure drop may be caused by the
364 filter housing design and by auxiliary elements of the filter, and this could potentially be
365 reduced without reducing the effectiveness of the filtration process (Bové et al., 2015).
366 From the CFD simulations, the velocity streamlines and pressures were analysed to
367 identify which regions of the filter housing caused most of the pressure drop. Figure 9
368 shows the results of the original filter housing simulated at $62.8 \text{ m}^3 \text{ h}^{-1}$ (i.e., mean flow
369 velocity at the inlet = 3.47 m s^{-1} , outlet pressure = 400 kPa). Eight lines were positioned
370 in the three-dimensional model, and the average pressure at each location was plotted
371 (Fig. 9A). The most critical regions in terms of pressure losses (i.e., regions i and ii) are
372 near the transitions between the inlet and outlet segments of the pipe (red dashed
373 rectangles in Fig. 9A). These regions present sudden expansion (i) and sudden
374 contraction (ii) of streamlines combined with the highest flow velocities (Fig. 9B). For
375 the simulated condition, 37.6% and 46.2% of the pressure drop in the filter housing
376 occurred from locations 2 to 3 (i.e., region i) and 5 to 6 (i.e., region ii), respectively
377 (Fig. 9A). Thus, 83.9% of the total pressure drop in the filter housing occurred at
378 regions i and ii. Improvements in filter housing seeking to reduce pressure losses should
379 focus on changing the dimensions near regions i and ii. Bové et al. (2015) showed the
380 importance of improving inlet/outlet regions and auxiliary elements of media filters.
381 These authors proposed a new underdrain design and a packing strategy that could
382 reduce the overall pressure drop in the filter by 35%.

383

[Fig. 9]

384 The filter inlet is left aligned in the filter housing, which leads to the vorticity and
385 circulation of water around the filter element. This position is important to avoid

386 excessive strain on a small region of the screen and to allow a better distribution of
387 impurities over the filtration element. A similar design of filter inlet was found for the
388 2” Spin Klin® disc filters – Amiad company (AMIAD, 2021).

389 In the current design of the filter housing, the highest flow velocities occurred at the
390 inlet and outlet of the filter housing (Fig. 9B), leading to most of the pressure losses.
391 The inlet and outlet sections should be enlarged to allow the filter to operate at higher
392 flow rates with feasible pressure losses.

393 While sizing pipelines for irrigation applications, mean flow velocities higher than 2.0 –
394 2.5 m s⁻¹ are not recommended for operation of pressurized systems (Azevedo Netto &
395 Fernandez, 2015; Frizzone et al., 2018; Lamm et al., 2007), but high velocities may
396 occur in short segments of pipes and in its components. In general, excessive flow
397 velocities increase pressure losses and energy waste, cause premature wear of
398 components, and lead to more intense pressure surges in the case of water hammer
399 events (Porto, 1999).

400 **3.3 Optimization of the filter housing dimensions**

401 The pressure losses in the filter housing designs simulated (Fig. 5) at 100 m³ h⁻¹ were: A
402 (80 mm) = 57.6 kPa; B (100 mm) = 35.8 kPa; C (125 mm) = 25.8 kPa; D (150 mm) =
403 13.3 kPa. Following the same schema of locations illustrated in Fig. 9, the pressure
404 losses were quantified for each of the proposed designs (Fig. 10). Increasing the
405 dimensions at the inlet and outlet segments of the pipe (i.e., at the critical regions i and
406 ii) effectively decreased the pressure drop in the filter housing. Because the allowable
407 pressure drop in a clean strainer-type filter should be lower than 30 kPa (Pizarro
408 Cabello, 1996), only designs C (125 mm) and D (150 mm) comply with the allowable
409 pressure drop criterion at the target flow rate of 100 m³ h⁻¹ ($q = 375 \text{ m}^3 \text{ m}^{-2} \text{ h}^{-1}$).

410

[Fig. 10]

411 A slight increase in pressure was observed between location 6 to 7 (Fig. 10). Although
412 such small values are not relevant for practical purposes, it is known that pressure
413 recovery downstream a 90° bend can be related to conversion between kinetic head and
414 pressure head. A bend or curve in a pipe, as in the filter outlet, induces a pressure loss
415 due to flow separation on the curved walls and a swirling secondary flow arising from
416 the centripetal acceleration (White, 2011).

417 **3.4 Filter housing designs combined with filter elements**

418 CFD simulations combining filter housing designs with woven and non-woven filter
419 elements were not possible in our current facilities. The arrangement, shape, and
420 dimensions of the fibres in each type of filter element would result in a highly complex
421 three-dimensional model that could not be simulated using the CFD module of
422 COMSOL Multiphysics. Further investigation may take advantage of simulation tools
423 such as GeoDict® filtration package, which has been developed particularly for the
424 simulation of air and liquid filtration processes using woven and non-woven fabrics and
425 meshes.

426 The experimental pressure drop equation shown in Table 2 assumes that the flow
427 pattern obtained without the filter element (i.e., only the filter housing) is the same than
428 that including it. But from Fig. 1, the installation of the filter element will modify the
429 flow pattern, mainly at the filter inlet. Although flow behaviour and minor losses are
430 influence by the presence of the filter element, the screen characteristics can be assumed
431 to be the dominant factor when summing the pressure drop of the filter housing and
432 filter element. A feasible method for approximating the pressure drop of the proposed
433 filter designs and the existing filter elements consists of summing the pressure drop of
434 each filter housing obtained from CFD with the pressure drop calculated from the
435 equations of filter elements shown in Table 2. At this stage, simplifications and

436 approximations must be performed to provide useful information before building new
 437 prototypes of the filter.
 438 The best size of the filter housing depends on which is the target nominal flow rate
 439 defined by the manufacturer according to market strategies. Assuming a target flow rate
 440 of $100 \text{ m}^3 \text{ h}^{-1}$, Table 3 presents estimated operational characteristics of the filter housing
 441 designs equipped with the filter elements. The total pressure drop (Δp_{total}) was
 442 estimated by summing the pressure drop caused by the filter element (Δp_f) and the
 443 pressure drop in the filter housing, which was obtained from the CFD simulations.

444 **Table 3.** Estimated operational characteristics of the filter housing designs equipped
 445 with filter elements operating at $100 \text{ m}^3 \text{ h}^{-1}$

Filter element	Δp_f (kPa)	Model of filter housing			
		A (80 mm)	B (100 mm)	C (125 mm)	D (150 mm)
		Δp_{total} (kPa)			
SS-120	7.9	65.5	43.7	33.7	21.2
SS-150	8.9	66.5	44.7	34.7	22.2
PP-120	6.8	64.4	42.6	32.6	20.1
NW-500	17.6	75.2	53.4	43.4	30.9
NW-2500	21.3	78.9	57.1	47.1	34.6

446
 447 Model A (80mm) corresponds to the original filter housing coupled to inlet and outlet
 448 pipes of 150 mm diameter by reducing adapters (Fig. 5A). From Table 3, improvements
 449 in terms of pressure drop reduction for operation at $100 \text{ m}^3 \text{ h}^{-1}$ can be observed. Taking
 450 the model A as the reference for comparisons, for the filter equipped with the element
 451 SS-120, the decrease in pressure drop was 33.3, 48.5 and 67.6% for the designs B, C
 452 and D, respectively. For NW-2500, which presents the smallest permeability among the
 453 evaluated elements, the decrease in pressure drop was 27.6, 40.3 and 56.1% for the
 454 designs B, C and D, respectively.

455 In general, the woven wire filter elements (i.e., SS-120, SS-150, and PP-120) mounted
456 within the filter housing D (150 mm) could operate at flow rates up to $100 \text{ m}^3 \text{ h}^{-1}$ with
457 pressure drop lower than 30 kPa, which is a threshold mentioned by Pizarro Cabello
458 (1996). Even the model C (125 mm) could be suitable since its values of Δp_{total} are
459 near 30 kPa. Although the evaluation of the efficiency of suspended solids removal is
460 not part of this research, the filtration efficiency is acceptable because the filtration rate
461 values are matching the thresholds of commercial screen filters.

462 The obtained results provide useful information for planning enhancements of the
463 filtration system and for building prototypes for further experimental evaluation.

464 **4 CONCLUSIONS**

465 The hydraulic performance and flow behavior of an automatic flushing strainer-type
466 filter operated with clean water were investigated using experimental and numerical
467 approaches. For the original filtration system equipped with woven elements, the
468 experimental results indicated that the pressure drop due to the filter housing was
469 dominant and represented more than 86% of the total pressure drop in the filtering
470 system. Similarly, for non-woven elements, more than 53% of the total pressure drop
471 was caused by the filter housing. Excessive pressure drop in the filter housing and low
472 filtration rates were identified as the main opportunities for improving the original
473 filtration system.

474 CFD simulations were performed to predict values of pressure drop of the original filter
475 housing operated with clean water. Numerical simulations enabled the identification of
476 the most critical regions in terms of pressure losses near the transitions between the inlet
477 and outlet segments of the pipe.

478 Keeping the filtering area constant, four designs of filter housing were simulated to
479 evaluate possibilities for optimizing the filter housing dimensions. Larger inlet and

480 outlet diameters combined to a filter housing shorter and wider were improvements in
481 the filter housing dimensions that enabled to decrease the pressure drop in the filter
482 and/or increase the range of operating flow rates. When comparing the proposed models
483 of filter housing (models B, C and D) against the original design (model A) at the flow
484 rate of $100 \text{ m}^3 \text{ h}^{-1}$ (i.e., filtration rate of $375 \text{ m}^3 \text{ m}^2 \text{ h}^{-1}$), the decrease in pressure drop
485 varied from 27.6% to 67.6% according to the combination of filter element and model
486 of filter housing.

487 The CFD simulations indicates that the filter housing design of an existing automatic
488 strainer-type filter can be improved to reduce pressure loss and/or increase the range of
489 operating flow rates. The obtained results provide useful information for planning
490 enhancements of the filtration system and for building prototypes for further
491 experimental evaluation. The best size of the filter housing depends on the target
492 nominal flow rate, which is defined by the manufacturer according to their market
493 strategies. For development purposes, numerical simulations may reduce the number of
494 prototypes manufactured for preliminary evaluations, thereby decreasing investment,
495 time, and labour requirements.

496 **5 ACKNOWLEDGEMENT**

497 The authors would like to thank the Fundação de Amparo à Pesquisa do Estado de São
498 Paulo [FAPESP-Brazil, Project 2018/20099-5] and Fundo de Apoio ao Ensino, Pesquisa
499 e Extensão of the Universidade Estadual de Campinas [FAEPEX/UNICAMP Project
500 No. 2022/19] for the financial support. We also appreciate the support of the Brazilian
501 company IAVANT Sistemas de Filtragem for providing the equipment used in this
502 investigation.

503 **6 REFERENCES**

504 AMIAD. (2021). *Spin Klin disc filter - AMIAD*. <https://amiad.com/wp->

505 content/uploads/2020/06/2-Spin-Klin-Catalogue-Irr-EN.pdf. Accessed on
506 10.02.2022

507 AMIAD. (2022). *Filtomat self-cleaning screen filter*. [https://amiad.com/wp-](https://amiad.com/wp-content/uploads/2020/06/Filtomat_A4_Irrig_En_2021-1.pdf)
508 content/uploads/2020/06/Filtomat_A4_Irrig_En_2021-1.pdf. Accessed on
509 10.02.2022

510 Arbat, G., Pujol, T., Montoro, L., Puig-Bargués, J., Duran-Ros, M., Barragán, J., & de
511 Cartagena, F. (2011). Using Computational Fluid Dynamics to Predict Head
512 Losses in the Auxiliary Elements of a Microirrigation Sand Filter. *Transactions of*
513 *the ASABE*, 54(4), 1367–1376. <https://doi.org/10.13031/2013.39038>

514 ASABE. (2017). *Media filters for irrigation - Testing and performance reporting -*
515 *ASAE S539 (R2017)*.

516 Azevedo Netto, J. M., & Fernandez, M. F. (2015). *Manual de hidráulica* (9th ed.). São
517 Paulo: Blucher.

518 AZUD. (2022). *Azud Luxon MFH*. [https://azud.com/wp-](https://azud.com/wp-content/uploads/2019/04/AZUD_LUXON_MFH-ENG.pdf)
519 content/uploads/2019/04/AZUD_LUXON_MFH-ENG.pdf. Accessed on
520 10.02.2022

521 Bové, J., Arbat, G., Duran-Ros, M., Pujol, T., Velayos, J., Ramírez de Cartagena, F., &
522 Puig-Bargués, J. (2015). Pressure drop across sand and recycled glass media used
523 in micro irrigation filters. *Biosystems Engineering*, 137, 55–63.
524 <https://doi.org/10.1016/j.biosystemseng.2015.07.009>

525 Bové, J., Arbat, G., Pujol, T., Duran-Ros, M., Ramírez de Cartagena, F., Velayos, J., &
526 Puig-Bargués, J. (2015). Reducing energy requirements for sand filtration in
527 microirrigation: Improving the underdrain and packing. *Biosystems Engineering*,
528 140, 67–78. <https://doi.org/10.1016/j.biosystemseng.2015.09.008>

529 Bové, J., Puig-Bargués, J., Arbat, G., Duran-Ros, M., Pujol, T., Pujol, J., & Ramírez de

530 Cartagena, F. (2017). Development of a new underdrain for improving the
531 efficiency of microirrigation sand media filters. *Agricultural Water Management*,
532 179, 296–305. <https://doi.org/10.1016/j.agwat.2016.06.031>

533 Camargo, A. P., Muniz, G. L., Cano, N. D., Ait-Mouheb, N., Tomas, S., Pereira, D. J.
534 de S., Lavanholi, R., Frizzone, J. A., & Molle, B. (2020). Applications of
535 computational fluid dynamics in irrigation engineering. *Revista Ciência*
536 *Agronômica*, 51(5). <https://doi.org/10.5935/1806-6690.20200097>

537 COMSOL Multiphysics. (2016). CFD Module User 's Guide. *COMSOL Multiphysics*,
538 598.
539 <https://doc.comsol.com/5.3/doc/com.comsol.help.cfd/CFDModuleUsersGuide.pdf>.
540 Accessed on 10.02.2022

541 Demir, V., Yürdem, H., Yazgi, A., & Değirmencioğlu, A. (2009). Determination of the
542 head losses in metal body disc filters used in drip irrigation systems. *Turkish*
543 *Journal of Agriculture and Forestry*, 33(3), 219–229. [https://doi.org/10.3906/tar-](https://doi.org/10.3906/tar-0811-1)
544 0811-1

545 Duran-Ros, M., Arbat, G., Barragán, J., Ramírez de Cartagena, F., & Puig-Bargués, J.
546 (2010). Assessment of head loss equations developed with dimensional analysis for
547 micro irrigation filters using effluents. *Biosystems Engineering*, 106(4), 521–526.
548 <https://doi.org/10.1016/j.biosystemseng.2010.06.001>

549 Frizzone, J. A., Rezende, R., Camargo, A. P., & Colombo, A. (2018). *Irrigação por*
550 *aspersão: sistema pivô central*. Maringá: UEM.

551 Ilker, P., & Sorgun, M. (2020). Performance of turbulence models for single phase and
552 liquid-solid slurry flows in pressurized pipe systems. *Ocean Engineering*, 214, 1–
553 12. <https://doi.org/10.1016/j.oceaneng.2020.107711>

554 ISO9644. (2008). *Agricultural irrigation equipment — Pressure losses in irrigation*

555 valves — *Test method*.

556 ISO9912-1. (2004). *Agricultural irrigation equipment — Filters for micro-irrigation —*
557 *Part 1: Terms, definitions and classification*.

558 ISO9912-3. (2013). *Agricultural irrigation equipment — Filters for microirrigation —*
559 *Part 3: Automatic flushing strainer-type filters and disc filters*.

560 Keller, J., & Bliesner, R. D. (2000). *Sprinkle and Trickle Irrigation*. Caldwell: The
561 Blackburn press.

562 Lamm, F. R., Ayars, J. E., & Nakayama, F. S. (2007). *Microirrigation for crop*
563 *production: design, operation and management*. Amsterdam: Elsevier.

564 Mesquita, M., Deus, F. P., Testezlaf, R., Rosa, L. M., & Diotto, A. V. (2019). Design
565 and hydrodynamic performance testing of a new pressure sand filter diffuser plate
566 using numerical simulation. *Biosystems Engineering*, 183, 58–69.
567 <https://doi.org/10.1016/j.biosystemseng.2019.04.015>

568 Mesquita, M., Testezlaf, R., Deus, F. P., & Rosa, L. M. (2017). Characterization of flow
569 lines generated by pressurized sand filter underdrains. *Chemical Engineering*
570 *Transactions*, 58, 715–720. <https://doi.org/10.3303/CET1758120>

571 Movahedi, H., & Jamshidi, S. (2021). Experimental and CFD simulation of slurry flow
572 in the annular flow path using two-fluid model. *Journal of Petroleum Science and*
573 *Engineering*, 198, 1–19. <https://doi.org/10.1016/j.petrol.2020.108224>

574 Nakayama, F. S., Boman, B. J., & Pitts, D. J. (2007). Maintenance. In F.R. Lamm, J. E.
575 Ayars, & F. S. Nakayama (Eds.), *Microirrigation for Crop Production* (pp. 389–
576 430). Amsterdam: Elsevier.

577 NETAFIM. (2022). *Screenguard™ automatic screen filters*.
578 [https://www.netafim.com/4ad930/globalassets/products/filters/screenguard/screeng](https://www.netafim.com/4ad930/globalassets/products/filters/screenguard/screenguard-automatic-screen-filter-product-page.pdf)
579 [uard-automatic-screen-filter-product-page.pdf](https://www.netafim.com/4ad930/globalassets/products/filters/screenguard/screenguard-automatic-screen-filter-product-page.pdf). Accessed on 10.02.2022

580 Oliveira, F. C., Lavanholi, R., Camargo, A. P., Ait-Mouheb, N., Frizzzone, J. A., Tomas,
581 S., & Molle, B. (2020). Clogging of drippers caused by suspensions of kaolinite
582 and montmorillonite clays. *Irrigation Science*, 38(1), 65–75.
583 <https://doi.org/10.1007/s00271-019-00652-4>

584 Pizarro Cabello, F. (1996). *Riegos localizados de alta frecuencia* (3rd ed.). Madrid:
585 Ediciones Mundi-Prensa.

586 Pope, S. B. (2000). *Turbulent flows*. Cambridge: Cambridge University Press.

587 Porto, R. M. (1999). *Hidráulica básica* (2nd ed.). São Carlos: EESC-USP.

588 Puig-Bargués, J., Barragán, J., & Ramírez de Cartagena, F. (2005). Development of
589 Equations for calculating the Head Loss in Effluent Filtration in Microirrigation
590 Systems using Dimensional Analysis. *Biosystems Engineering*, 92(3), 383–390.
591 <https://doi.org/10.1016/j.biosystemseng.2005.07.009>

592 Puig-Bargués, J., & Lamm, F. (2013). Effect of Flushing Velocity and Flushing
593 Duration on Sediment Transport in Microirrigation Driplines. *Transactions of the*
594 *ASABE*, 56(5), 1821–1828. <https://doi.org/10.13031/trans.56.10293>

595 Pujol, T., Puig-Bargués, J., Arbat, G., Duran-Ros, M., Solé-Torres, C., Pujol, J., &
596 Ramírez de Cartagena, F. (2020). Effect of wand-type underdrains on the hydraulic
597 performance of pressurised sand media filters. *Biosystems Engineering*, 192, 176–
598 187. <https://doi.org/10.1016/j.biosystemseng.2020.01.015>

599 Purchas, D. B., & Sutherland, K. (2002). *Handbook of Filter Media* (2nd ed.).
600 Amsterdam: Elsevier Science & Technology Books.

601 Ravina, I., Paz, E., Sofer, Z., Marcu, A., Shisha, A., & Sagi, G. (1992). Control of
602 emitter clogging in drip irrigation with reclaimed wastewater. *Irrigation Science*,
603 13(3), 129–139. <https://doi.org/10.1007/BF00191055>

604 Ravina, I., Paz, E., Sofer, Z., Marm, A., Schischa, A., Sagi, G., Yechialy, Z., & Lev, Y.

605 (1997). Control of clogging in drip irrigation with stored treated municipal sewage
606 effluent. *Agricultural Water Management*, 33, 127–137.
607 [https://doi.org/10.1016/S0378-3774\(96\)01286-3](https://doi.org/10.1016/S0378-3774(96)01286-3)

608 Ribeiro, T. A. P., Paterniani, J. E. S., Airoidi, R. P. S., & Silva, M. J. M. (2004).
609 Performance of non woven synthetic fabric and disc filters for fertirrigation water
610 treatment. *Scientia Agricola*, 61(2), 127–133. [https://doi.org/10.1590/S0103-](https://doi.org/10.1590/S0103-90162004000200001)
611 [90162004000200001](https://doi.org/10.1590/S0103-90162004000200001)

612 Ribeiro, T. A. P., Paterniani, J. E. S., Airoidi, R. P. S., & Silva, M. J. M. (2008).
613 Comparison Between Disc and Non-Woven Synthetic Fabric Filter Media to
614 Prevent Emitter Clogging. *Transactions of the ASABE*, 51(2), 441–453.
615 <https://doi.org/10.13031/2013.24386>

616 Solé-Torres, C., Puig-Bargués, J., Duran-Ros, M., Arbat, G., Pujol, J., & Ramírez de
617 Cartagena, F. (2019). Effect of underdrain design, media height and filtration
618 velocity on the performance of microirrigation sand filters using reclaimed
619 effluents. *Biosystems Engineering*, 187, 292–304.
620 <https://doi.org/10.1016/j.biosystemseng.2019.09.012>

621 Sparks, T., & Chase, G. (2016). *Filters and filtration handbook* (6th ed.). Waltham:
622 Elsevier.

623 Sutherland, K. (2008). *Filters and filtration handbook* (5th ed.). Burlington: Elsevier.

624 Tabatabaian, M. (2015). *CFD Module: Turbulent Flow Modeling*. New Delhi: Mercury
625 learning and information.

626 Testezlaf, R., & Ramos, J. P. S. (1995). Sistema automatizado para determinação de
627 perda de carga em filtros de tela e disco usados na irrigação localizada. *Pesquisa*
628 *Agropecuária Brasileira*, 30(8), 1079–1088.

629 White, F. M. (2011). *Fluid Mechanics* (7th ed.). New York: McGraw-Hill.

630 Wu, W., Chen, W. E. I., Liu, H., Yin, S., & Niu, Y. (2014). A new model for head loss
631 assessment of screen filters developed with dimensional analysis in drip irrigation
632 systems. *Irrigation and Drainage*, 63(4), 523–531. <https://doi.org/10.1002/ird.1846>

633 Yurdem, H., Demir, V., & Degirmencioglu, A. (2008). Development of a mathematical
634 model to predict head losses from disc filters in drip irrigation systems using
635 dimensional analysis. *Biosystems Engineering*, 100(1), 14–23.
636 <https://doi.org/10.1016/j.biosystemseng.2008.01.003>

637 Yurdem, H., Demir, V., & Degirmencioglu, A. (2010). Development of a mathematical
638 model to predict clean water head losses in hydrocyclone filters in drip irrigation
639 systems using dimensional analysis. *Biosystems Engineering*, 105(4), 495–506.
640 <https://doi.org/10.1016/j.biosystemseng.2010.02.001>

641 Zong, Q., Zheng, T., Liu, H., & Li, C. (2015). Development of head loss equations for
642 self-cleaning screen filters in drip irrigation systems using dimensional analysis.
643 *Biosystems Engineering*, 133, 116–127.
644 <https://doi.org/10.1016/j.biosystemseng.2015.03.001>

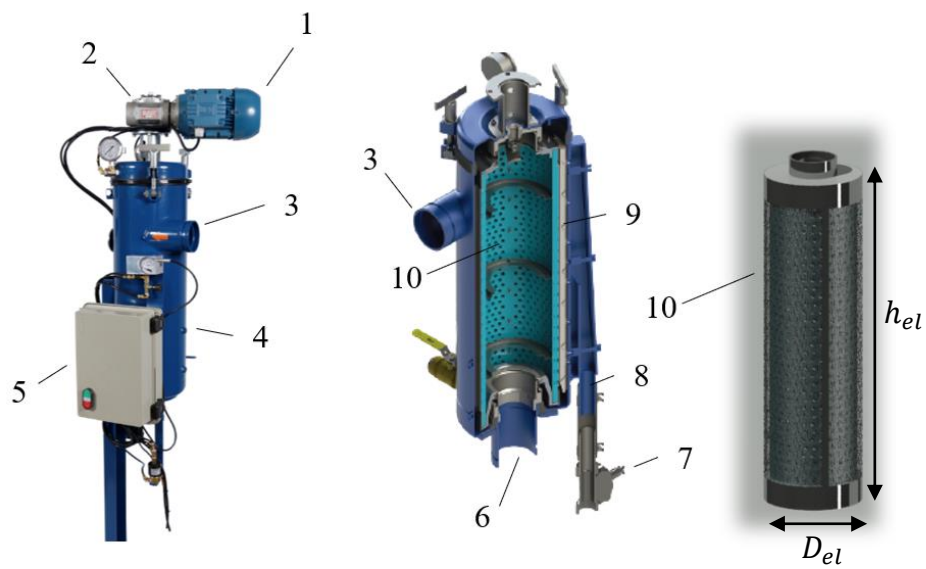


Fig. 1. Automatic flushing strainer-type filter model Iavant FA-20. (1: electric motor; 2: gearbox; 3: filter inlet; 4: filter housing; 5: control panel; 6: filter outlet; 7: flushing valve; 8: flushing pipe; 9: flushing cavity and brushes; 10: filter element; D_{el} : diameter of the filter element; h_{el} : diameter of the filter element)

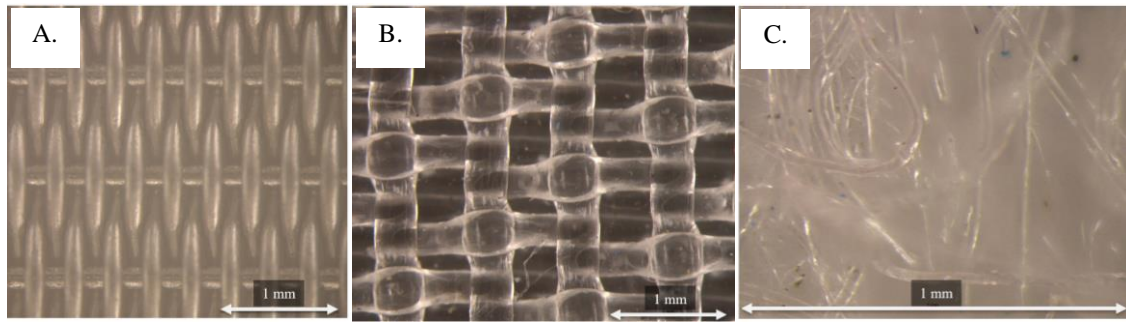


Fig. 2. Evaluated meshes: (A) stainless steel plain Dutch weave (SS-120 and SS-150); (B) polypropylene satim weave (PP-120); (C) non-woven needlona (NW-500 and NW-2500)

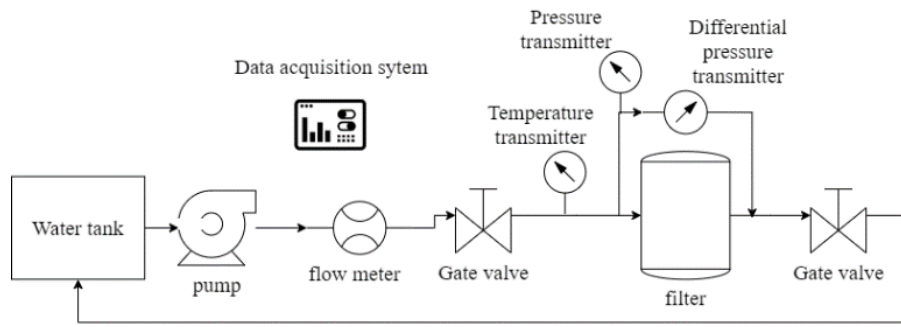


Fig. 3. Test bench diagram

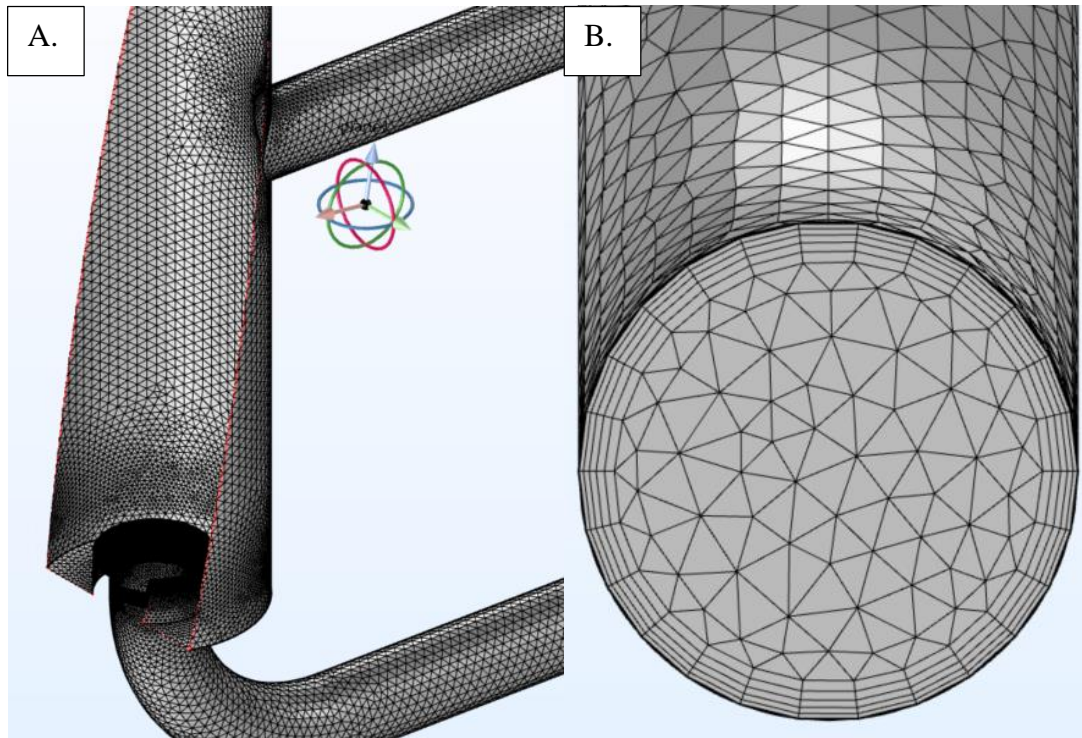


Fig. 4. Mesh generated based on free tetrahedrals (A) including a boundary layer mesh near the walls (B)

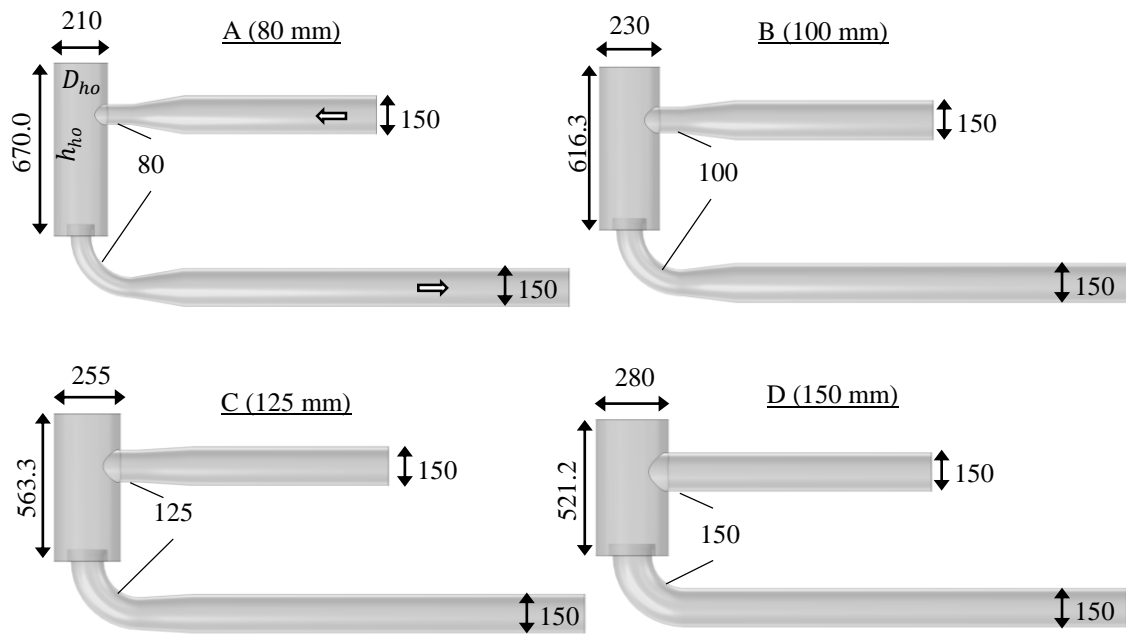
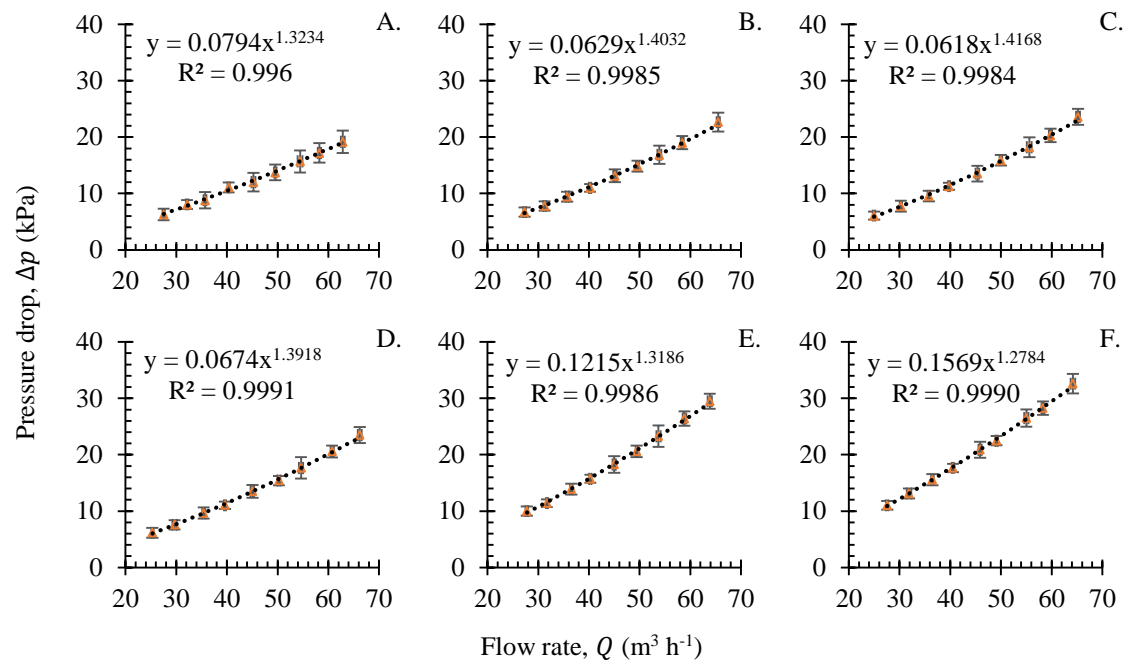


Fig. 5. Main dimensions of the four models of filter housing simulated (dimensions in mm)



*Error bars indicate the standard deviation

Fig. 6. Experimental results of pressure drop curves of the filter housing and the filtering system equipped with each of the filter elements. (A) filter housing; (B) SS-120; (C) SS-150; (D) PP-120; (E) NW-500; (F) NW-2500

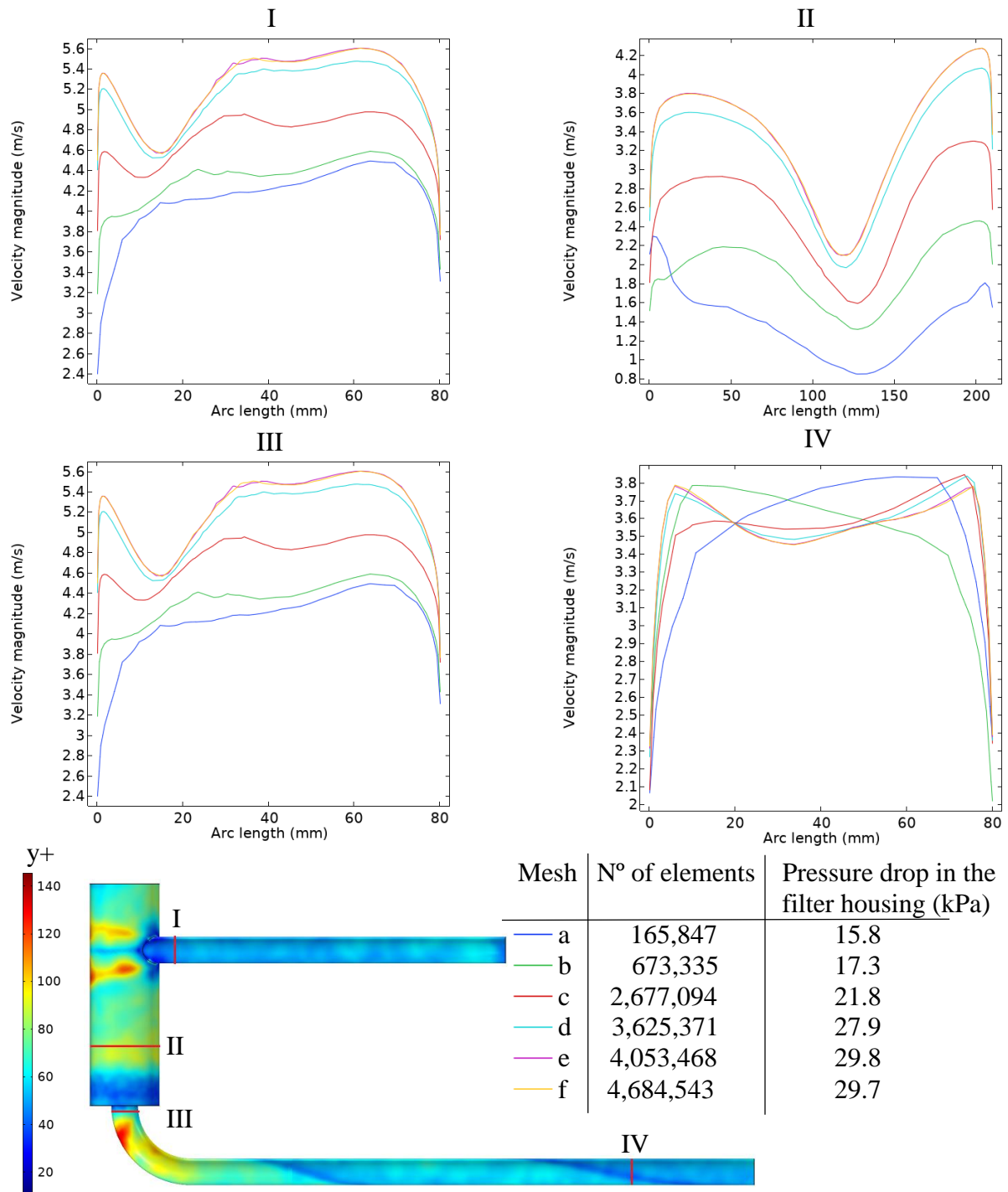


Fig. 7. Velocity profiles at four sections (I, II, III and IV) of the original filter housing operating at $62.8 \text{ m}^3 \text{ h}^{-1}$, pressure drop in the filter housing for each mesh size, and values of y^+ for mesh size “ f ” (4,684,543 elements) in which mesh independence of results was confirmed.

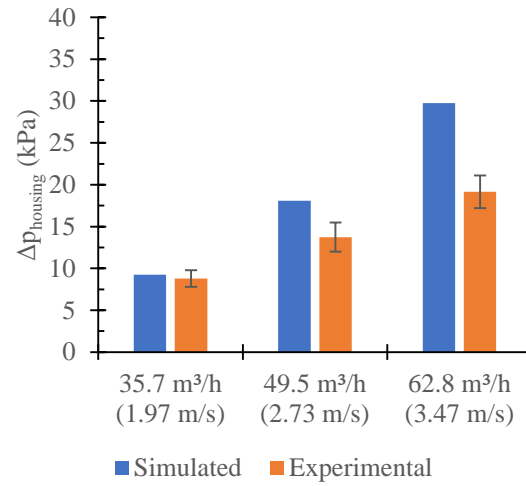
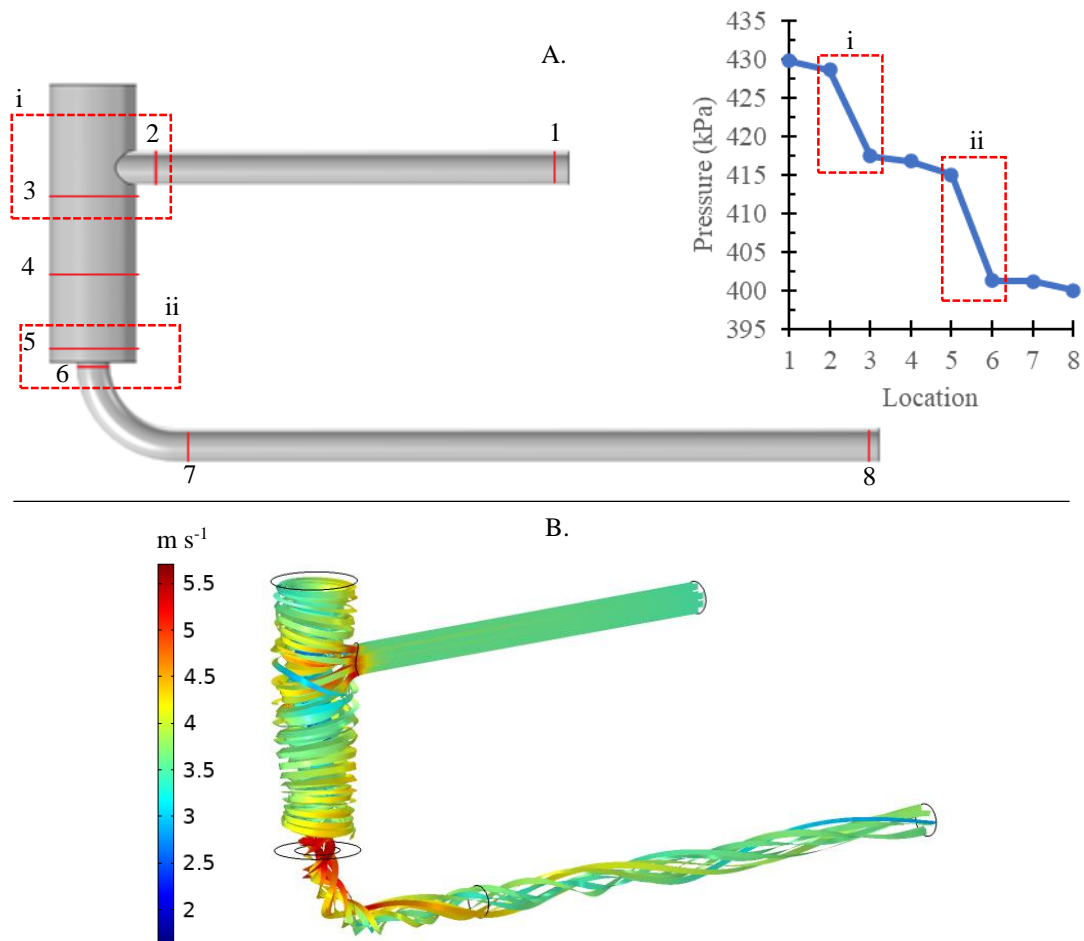


Fig. 8. Simulated vs experimental values of pressure drop for the original filter housing at three operating conditions of flow



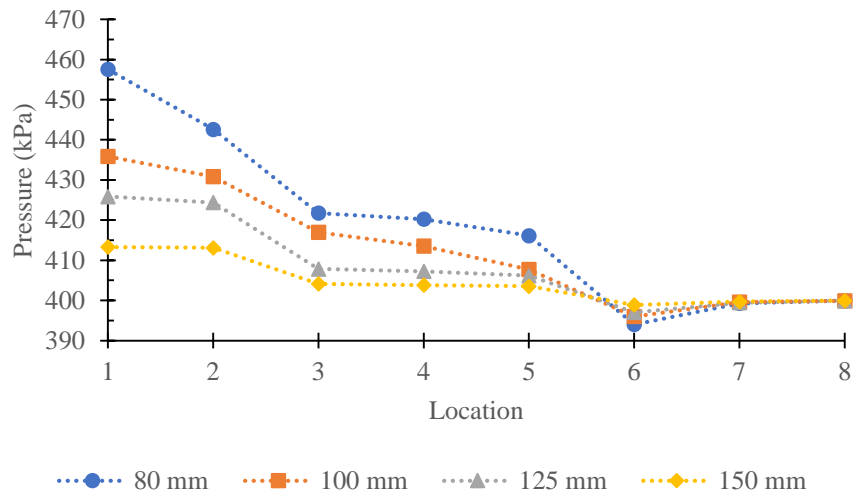


Fig. 10. Pressure losses of four designs of the filter housing simulated with a target flow $100 \text{ m}^3 \text{ h}^{-1}$ ($q = 375 \text{ m}^3 \text{ m}^{-2} \text{ h}^{-1}$)

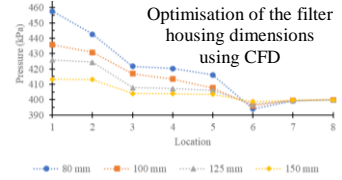
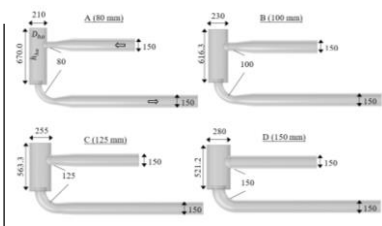
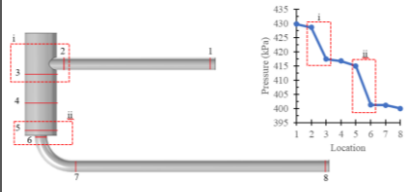
1

Graphical abstract (5 × 13 cm)

Automatic flushing strainer-type filter



Excessive pressure losses near inlet and outlet transitions



2

3

Response to the Editor

Editor comments: Thank you for making the changes required by the reviewers. Your paper is basically acceptable for publication but requires minor changes.

I have carried out a technical edit on your submission using Word Track Changes and suggested changes. You may access my edited version in the attachment. Please check my edits carefully as I may not have always understood your original meaning.

Please also check my comments.

I also suggest that you carefully examine the journal Instructions for Authors available through the journal web site.

I look forward to shortly receiving a revised manuscript and moving to accept it for publication.

Authors: Excellent news! Thank you very much.

- 1) *All your suggestions were accepted.*
- 2) *In Word software, the formatting option to justify text was modified. Now, all text is left aligned.*
- 3) *All references were corrected.*

If more improvements are necessary in the manuscript, please contact me.

Best regards

Antonio Pires de Camargo